# Supplementary Information for

# Hydrophobic ionic liquid and ZIF-8 co-modified graphene oxide membrane for efficient osmotic energy conversion

Yizhuo Wang,[a,b] Changchao Yan,[a,b] Jingyun Guo, [a,b] Zhizhen Ye,[a,b] Xinyi Wan*[a,b] and Xinsheng Peng*[a,b]

[a] State Key Laboratory of Silicon and Advanced Semiconductor Materials, School of Materials Science and Engineering, Zhejiang University, Hangzhou 310058, P. R. China.

[b] Wenzhou Key Laboratory of Novel Optoelectronic and Nanomaterials, Institute of Wenzhou, Zhejiang University, Wenzhou 325006, P. R. China.

* E-mail address: xinyi.wan@zju.edu.cn, pengxinsheng@zju.edu.cn

Content:

# Supplementary Notes

## Note S1 Calculation of ZIF-8 weight fraction in the GO/ZIF-8 composite membrane based on TGA results

The weight percentage of ZIF-8 in the GO/ZIF-8 composite membrane was calculated using the following two equations:

$$w_{\text{ZIF-8}} + w_{\text{GO}} = 1 \tag{1}$$

$$w_{\text{ZIF-8}} \times R_{\text{ZIF-8}} + w_{\text{GO}} \times R_{\text{GO}} = R_{\text{GO/ZIF-8}} \tag{2}$$

In this equation, $w_{\text{ZIF-8}}$ and $w_{\text{GO}}$ represent the weight percentages of ZIF-8 and GO in the GO/ZIF-8 composite membrane, respectively. $R_{\text{ZIF-8}}$, $R_{\text{GO}}$ and $R_{\text{GO/ZIF-8}}$ represent the residual weight percentages of ZIF-8 powder, GO membrane and GO/ZIF-8 composite membrane, respectively.

## Note S2 The interlayer spacing of membrane

The interlayer spacing ($d$) of the membrane can be calculated using Bragg's equation:[1]

$$2d \sin\theta = n\lambda \tag{3}$$

where $\lambda$ is the wavelength of the incident wave (1.54 Å), $\theta$ is the angle between the incident wave and the scattering.

## Note S3 The surface charge density of membrane

According to the electrical double layer (EDL) theory, the Debye length ($\lambda_{\text{D}}$) represents the characteristic scale over which the surface potential decays in solution due to ionic screening, and it can be estimated by the following equation:[2]

$$\lambda_{\text{D}} = \sqrt{\frac{\varepsilon_{\text{r}}\varepsilon_0 K_{\text{B}} T}{e^2 N_{\text{A}} \sum_i c_i z_i^2}} \tag{4}$$

where $\varepsilon_{\text{r}}$ and $\varepsilon_0$ stand for the relative permittivity of solution and vacuum permittivity, respectively. $K_{\text{B}}$ is the Boltzmann constant, $T$ is the absolute temperature, $e$ is the electron charge, $N_{\text{A}}$ is the Avogadro constant, $c$ is the concentration, and $z$ is the ionic valence. Based on the measured zeta potential, the surface charge density ($\sigma_{\text{s}}$) of membrane can be calculated using

the following equation:

$$\sigma_s = \frac{\varepsilon_r \varepsilon_0 \zeta}{\lambda_D} \tag{5}$$

where $\zeta$ is the zeta potential. The zeta potentials of GO/ZIF-8 and GO/ZIF-8/[Bmim][$NTf_2$] composite membranes are −35.8 and −70.9 mV, respectively. Based on the above equations, the Debye length in 0.01 M KCl solution is calculated to be approximately 3.04 nm. Furthermore, the surface charge densities of GO/ZIF-8 and GO/ZIF-8/[Bmim][$NTf_2$] composite membranes are estimated to be −0.008 and −0.016 C $m^{-2}$, respectively.

**Note S4 Electrode calibration**

The measured open-circuit voltage ($V_{oc}$) consists of two components: the diffusion potential ($E_{diff}$) and the redox potential ($E_{redox}$), where $E_{diff}$ arises from the ion selectivity of membrane, leading to different diffusion rates of anions and cations, whereas $E_{redox}$ results from the difference in concentrations of redox-active species in the solutions on both sides of membrane, generating a potential difference at the electrode surfaces.[3] The corresponding equivalent circuit is shown in Fig. S8. In this work, the contribution of $E_{redox}$ was determined experimentally. A non-selective silicon membrane containing a single micro-window was used to replace the nanofluidic membrane, under such condition the measured $V_{oc}$ was solely attributed to $E_{redox}$. By subtracting the contribution of $E_{redox}$ through electrode calibration, $E_{diff}$ was obtained, as calculated by the following equation:

$$E_{diff} = V_{oc} - E_{redox} \tag{6}$$

**Note S5 Cation transference number and Energy conversion efficiency**

The cation transference number ($t_+$) of membrane was quantified by calculating the $Na^+$ transference under the corresponding concentration gradient using the Nernst equation, as expressed by the following formula:

$$t_+ = \frac{1}{2}\left( \frac{E_{diff}}{\frac{RT}{zF}\ln\left(\frac{\gamma_H C_H}{\gamma_L C_L}\right)} + 1 \right) \quad (7)$$

Here, $\gamma$ and $C$ stand for the ion activity coefficient and the concentration, respectively. Moreover, $R$ is the universal gas constant, $T$ is the absolute temperature, $z$ indicates the ionic valence, and $F$ denotes the Faraday constant. The energy conversion efficiency ($\eta$) was calculated from the $t_+$, as expressed by the following equation:

$$\eta = \frac{1}{2}\left(2t_+ - 1\right)^2 \quad (8)$$

The obtained $I_{sc}$, $V_{oc}$, $E_{redox}$, $E_{diff}$, $t_+$ and $\eta$ of GO membrane, GO/ZIF-8 composite membrane and GO/ZIF-8/[Bmim][$NTf_2$] composite membrane are shown in Tables S2-S4.

**Note S6 Theoretical calculation based on Poisson-Nernst-Planck (PNP) equations**

The ion transport behavior of GO/ZIF-8/[Bmim][$NTf_2$] composite membrane was theoretically investigated using the commercial finite element software COMSOL Multiphysics. A continuum model based on the PNP equations was established to simulate the steady-state ion concentration distribution within the nanofluidic channels.[4] The contributions of diffusion current driven by the concentration gradient, and migration current driven by the potential gradient, to the overall ionic flux were described by the Nernst–Planck equation:

$$J_i = D_i\left(\nabla c_i + \frac{z_i F c_i}{RT}\nabla\varphi\right) \quad (9)$$

where $J_i$, $D_i$, $c_i$, $z_i$, $F$, $R$, $T$ and $\varphi$ represents the ionic flux, diffusion coefficient, ion concentration, valence number, Faraday constant, universal gas constant, absolute temperature and electrical potential, respectively. The diffusion coefficients of cations and anions were set to be $1.334\times10^{-9}$ $m^2$ $s^{-1}$ and $2.032\times10^{-9}$ $m^2$ $s^{-1}$, respectively.[错误!未找到引用源。] The relationship between electric potential and ion concentration follows the Poisson equation:

$$\nabla^2\varphi = -\frac{F}{\varepsilon}\sum z_i c_i \quad (10)$$

where $\varepsilon$ stands for the dielectric constant of salt solutions. The system is generally simplified by assuming steady-state conditions. In this case, the ionic flux is required to satisfy the

following equation:

$$\nabla J_i = 0 \tag{11}$$

The boundary condition for the electrical potential on the channel wall is:

$$\vec{n} \times \nabla \varphi = -\frac{\sigma}{\varepsilon} \tag{12}$$

where $\sigma$ is the surface charge density. The normal component of the ionic flux at the boundary is zero:

$$\vec{n} \times J_i = 0 \tag{13}$$

As shown in Fig. S18, the computational models of GO/[Bmim][$NTf_2$] channel and GO/ZIF-8/[Bmim][$NTf_2$] channel were constructed. To achieve a computationally feasible scale, the system was simplified by neglecting the heterogeneity of chemical composition, porous structure and charge distribution, aiming to capture the essential physical scenario rather than to quantitatively reproduce the experimental results. Specifically, the GO/[Bmim][$NTf_2$] was simplified to a 2D single channel with a length of 100 nm and a diameter of 5 nm. In contrast, the GO/ZIF-8/[Bmim][$NTf_2$] was modeled as a hybrid nanochannel, where the ZIF-8 segment had a length of 10 nm and a diameter of 1.1 nm, while the GO segment had a length of 90 nm and a diameter of 5 nm. To reduce the influence of mass transfer resistance at the inlet and outlet, two electrolyte reservoirs with dimensions of 100 × 50 nm were added at both ends, containing NaCl solutions with concentration gradient of 50-fold (0.5 M/0.01 M). The surface charge density of channels was set to −0.02 C $m^{-2}$, which is a reasonable value for typical nanofluidic materials.[5]

## Supplementary Figures

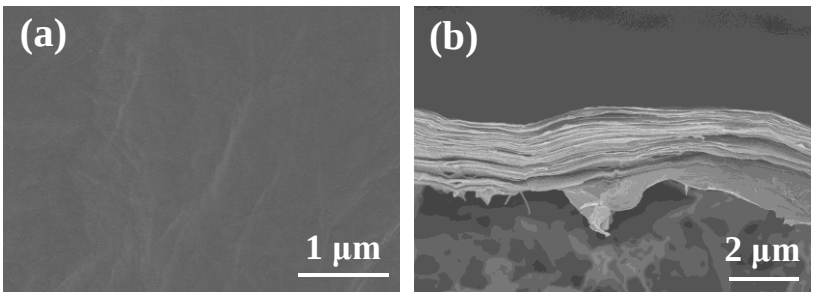


**Fig. S1** The surface (a) and cross-section (b) SEM images of GO membrane.

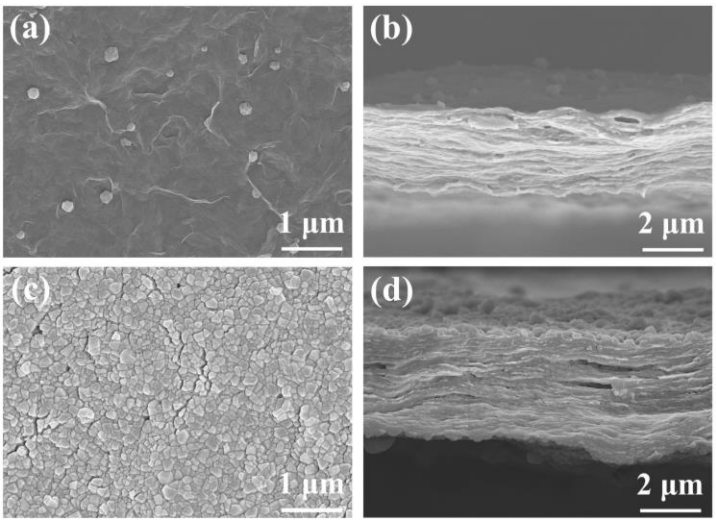


**Fig. 2** The surface and cross-section SEM images of GO/ZIF-8 composite membrane with different volume of ZHNs solution: 5 mL (a and b) and 15 mL (c and d).

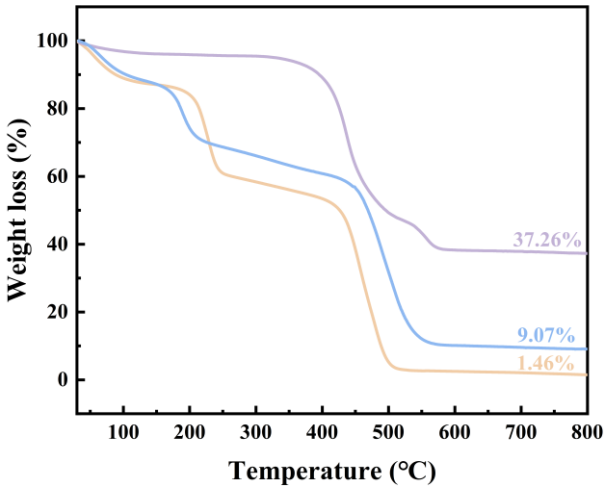


**Fig. S3** The TGA curves of GO membrane, ZIF-8 and GO/ZIF-8 composite membrane.

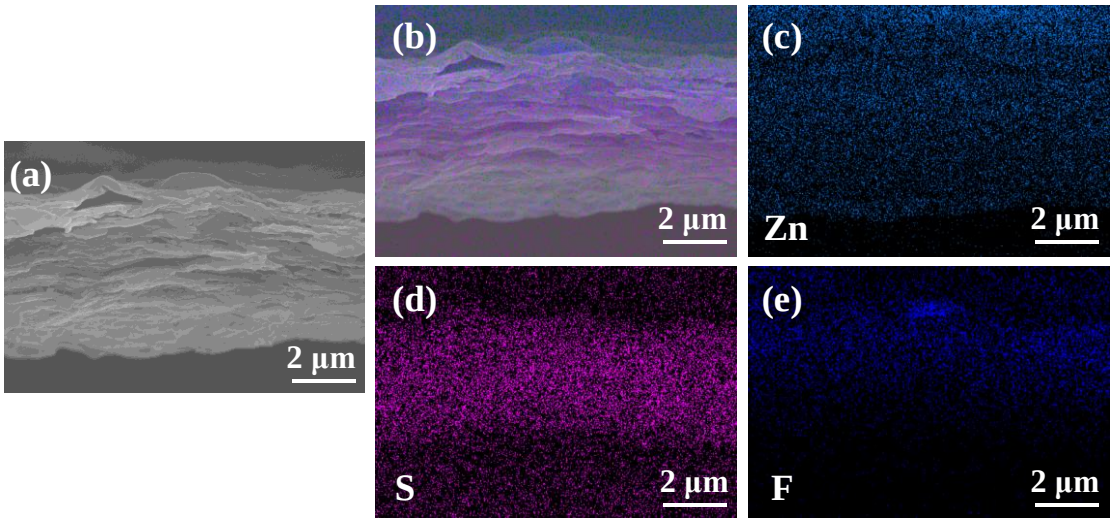


**Fig. S4** The cross-section SEM image (a) and corresponding EDS elemental mappings (b–e) of GO/ZIF-8/[Bmim][$NTf_2$] composite membrane.

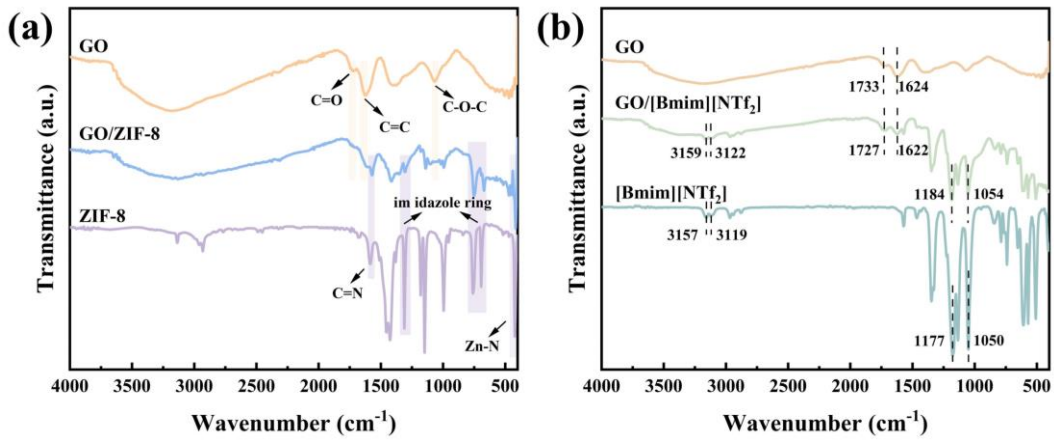


**Fig. S5** (a) The ATR–FTIR spectra of GO membrane, ZIF-8 and GO/ZIF-8 composite membrane. (b) The ATR–FTIR spectra of GO membrane, [Bmim][$NTf_2$] and GO/[Bmim][$NTf_2$] membrane.

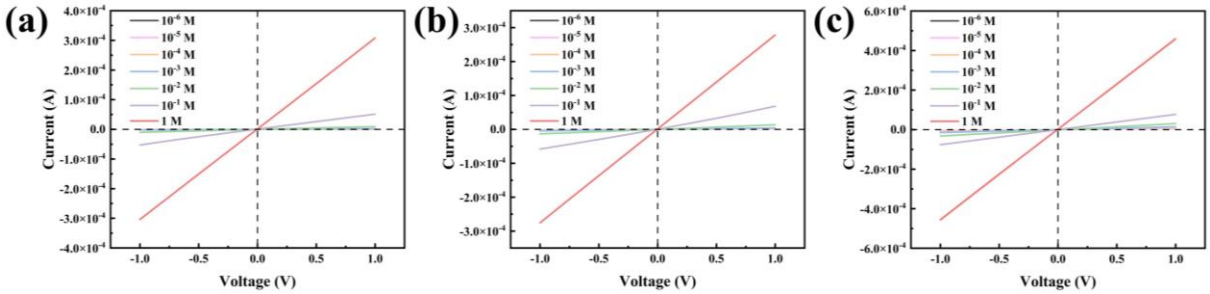


**Fig. S6** The *I–V* curves of (a) GO membrane, (b) GO/ZIF-8 composite membrane and (c) GO/ZIF-8/[Bmim][$NTf_2$] composite membrane under different concentrations of KCl electrolyte solution.

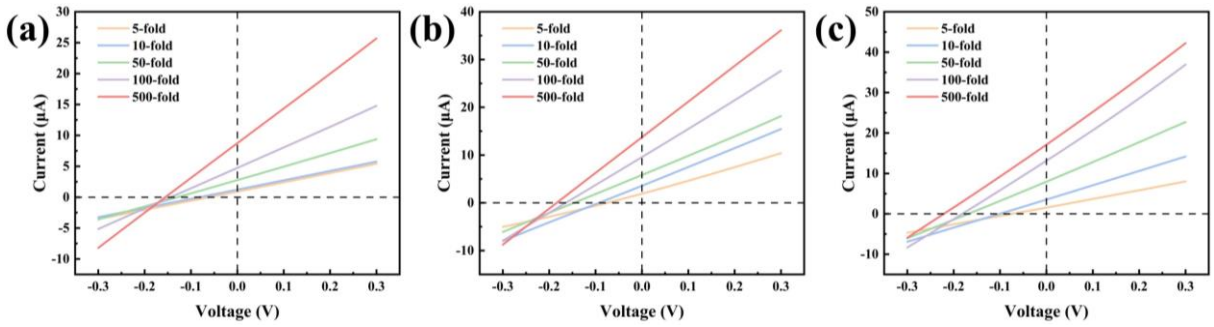


**Fig. S7** The *I–V* curves of (a) GO membrane, (b) GO/ZIF-8 composite membrane and (c) GO/ZIF-8/[Bmim][$NTf_2$] composite membrane under a series of NaCl concentration gradients. The concentration on the low-concentration side was fixed at 0.01 M, while the high-concentration side varied from 0.05 M to 5 M.

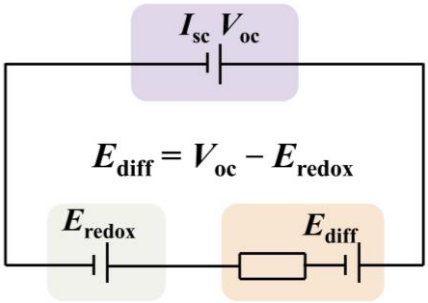


**Fig. S8** The equivalent circuit of membrane-based power generator.

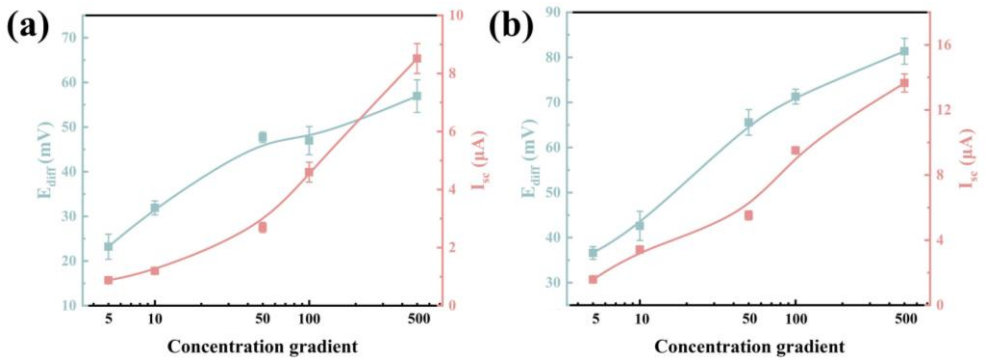


**Fig. S9** The $E_{diff}$ and $I_{sc}$ of (a) GO membrane and (b) GO/ZIF-8 composite membrane under different NaCl concentration gradients.

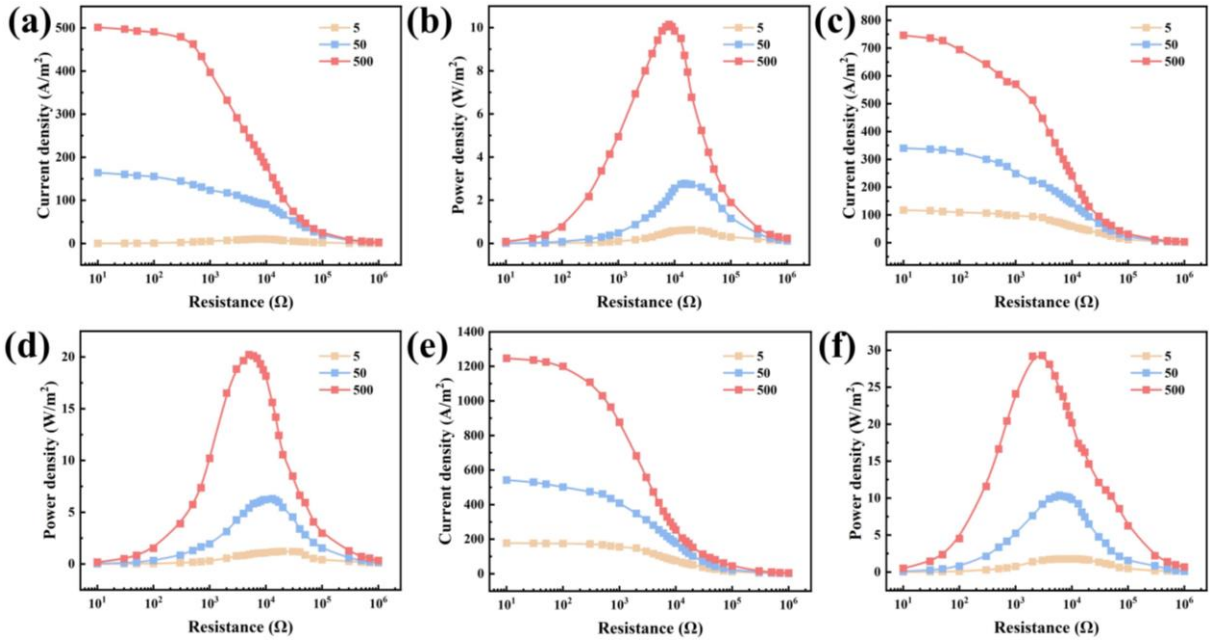


**Fig. S10** The current densities and power densities of (a,b) GO membrane, (c,d) GO/ZIF-8 composite membrane and (e,f) GO/ZIF-8/[Bmim][$NTf_2$] composite membrane with different external resistances under different NaCl concentration gradients.

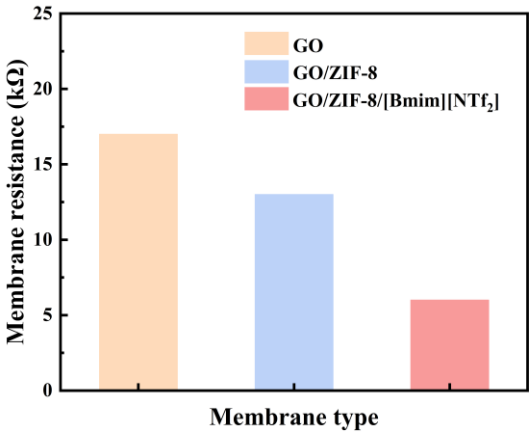


**Fig. S11** The internal resistances of GO membrane, GO/ZIF-8 composite membrane and GO/ZIF-8/[Bmim][$NTf_2$] composite membrane under 50-fold NaCl concentration gradient.

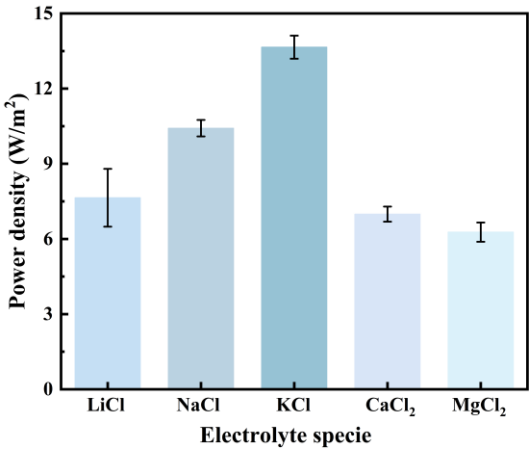


**Fig. S12** The power densities of GO/ZIF-8/[Bmim][$NTf_2$] composite membrane in different chloride salt solutions.

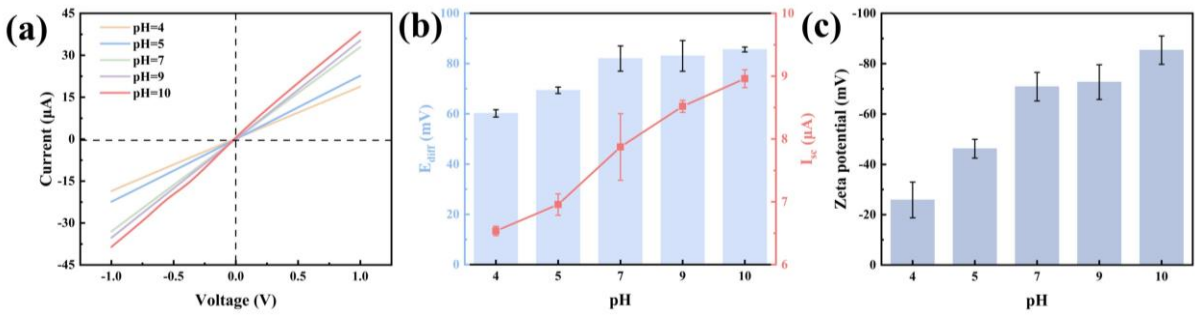


**Fig. S13** (a) The *I–V* curves of GO/ZIF-8/[Bmim][$NTf_2$] composite membrane in 0.01 M KCl electrolyte solution with different pH values. (b) The $E_{diff}$ and $I_{sc}$ of GO/ZIF-8/[Bmim][$NTf_2$] composite membrane under 50-fold NaCl concentration gradient with different pH values. (c) The zeta potential of GO/ZIF-8/[Bmim][$NTf_2$] composite membrane under different pH values.

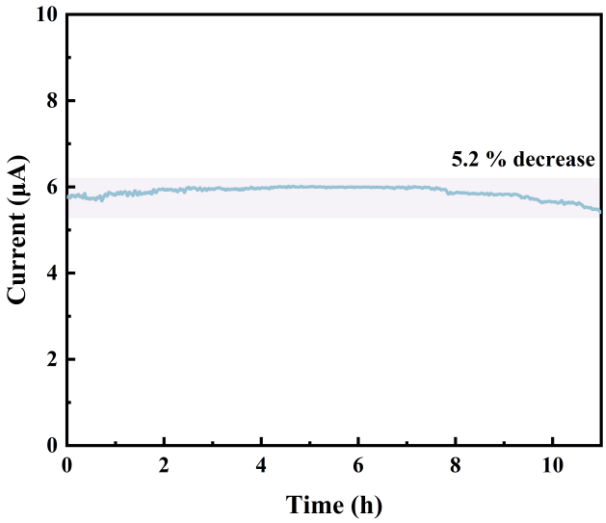


**Fig. S14** The long-term stability of GO/ZIF-8/[Bmim][$NTf_2$] composite membrane under 50-fold NaCl concentration gradient.

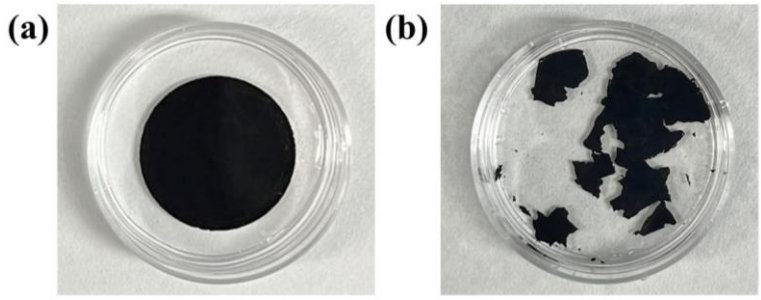


**Fig. S15** The digital photographs of (a) GO/ZIF-8/[Bmim][$NTf_2$] composite membrane and (b) GO/ZIF-8 composite membrane after testing in 0.5 M NaCl solution for 10 days.

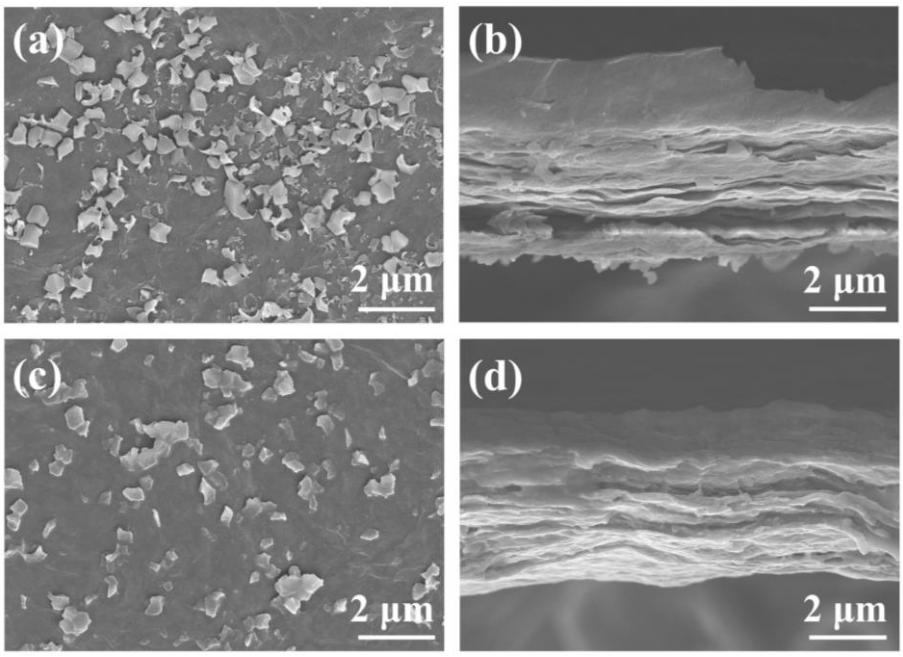


**Fig. S16** The surface and cross-section SEM images of GO/ZIF-8 composite membrane (a and b) and GO/ZIF-8/[Bmim][$NTf_2$] composite membrane (c and d) after testing in 0.5 M NaCl solution for 11 h.

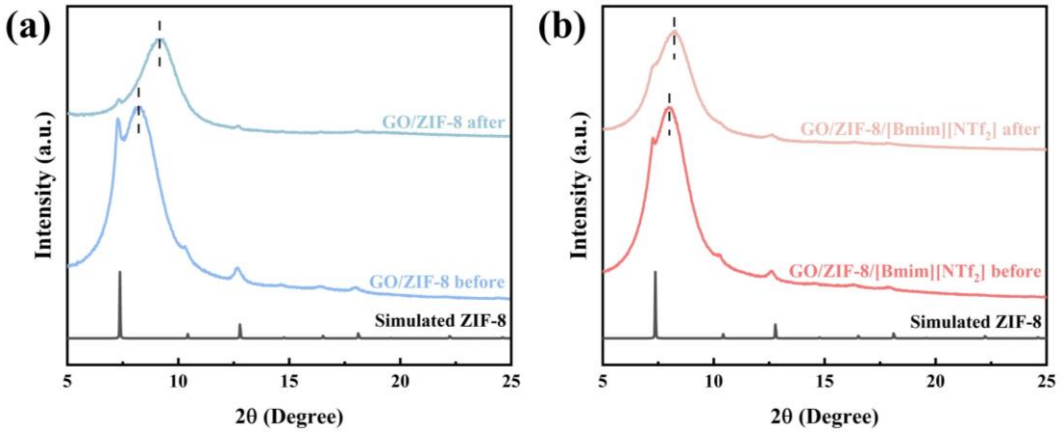


**Fig. S17** The XRD patterns of (a) GO/ZIF-8 composite membrane and (b) GO/ZIF-8/[Bmim][$NTf_2$] composite membrane before and after testing in 0.5 M NaCl solution for 11 h.

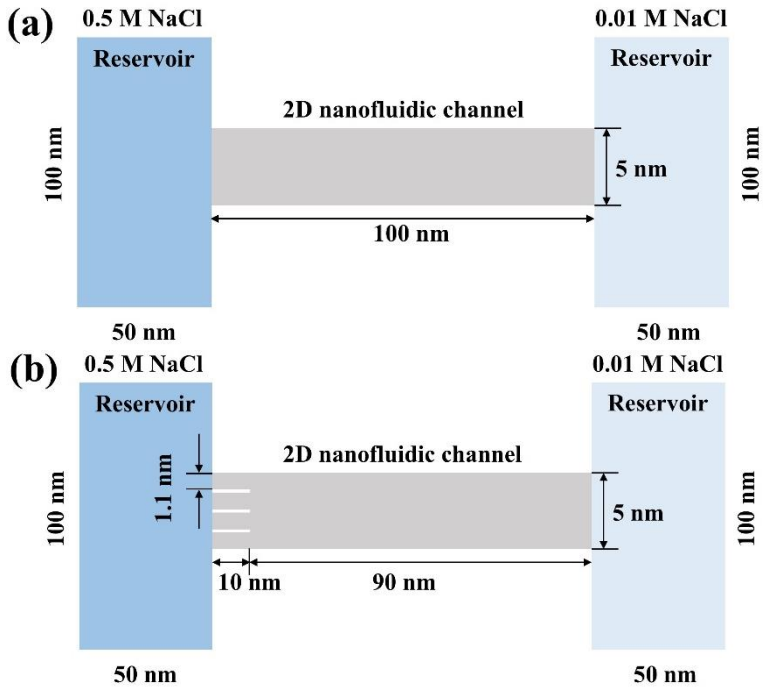


**Fig. S18** Schematic illustration of the simplified PNP simulation models showing (a) GO/[Bmim][$NTf_2$] channel and (b) GO/ZIF-8/[Bmim][$NTf_2$] channel (drawing not to scale).

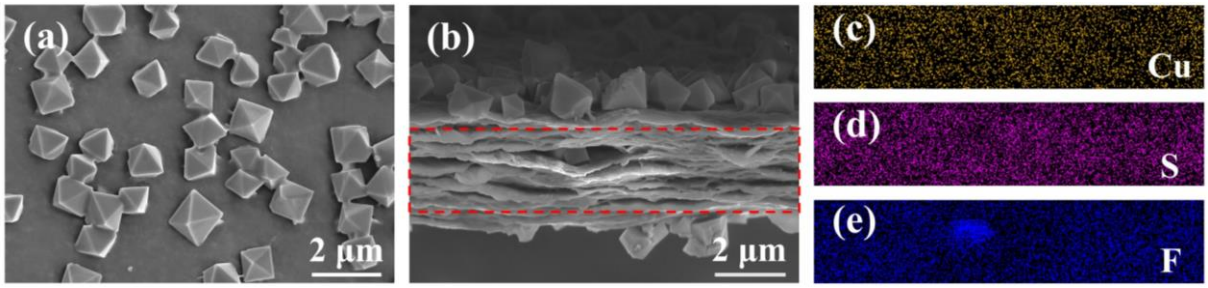


**Fig. S19** The surface (a) and cross-section (b) SEM images of GO/HKUST-1/[Bmim][$NTf_2$] composite membrane. The element mapping images of (c) Cu, (d) S and (e) F of the marked section zone in (b).

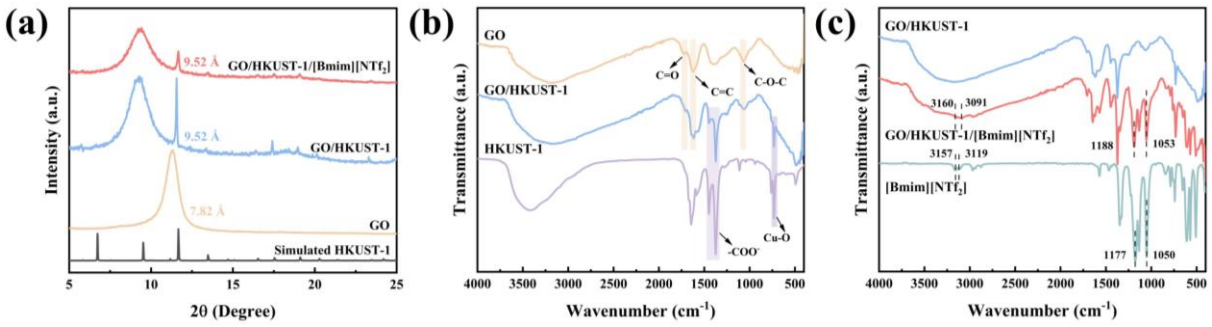


**Fig. S20** (a) The XRD patterns of GO membrane, GO/HKUST-1 composite membrane and GO/HKUST-1/[Bmim][$NTf_2$] composite membrane. The XRD results confirm the successful incorporation of HKUST-1 and [Bmim][$NTf_2$]. (b) The ATR–FTIR spectra of GO membrane, HKUST-1 and GO/HKUST-1 composite membrane. (c) The ATR–FTIR spectra of GO/HKUST-1 composite membrane, [Bmim][$NTf_2$] and GO/HKUST-1/[Bmim][$NTf_2$] composite membrane.

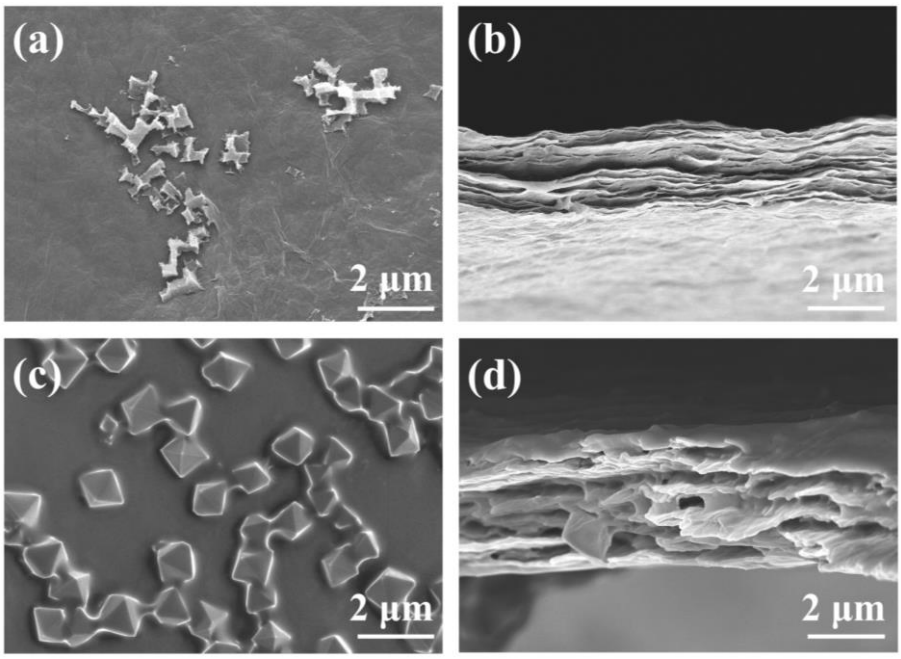


**Fig. S21** The surface and cross-section SEM images of GO/HKUST-1 composite membrane (a and b) and GO/HKUST-1/[Bmim][$NTf_2$] composite membrane (c and d) after testing in 0.5 M NaCl solution for 11 h.

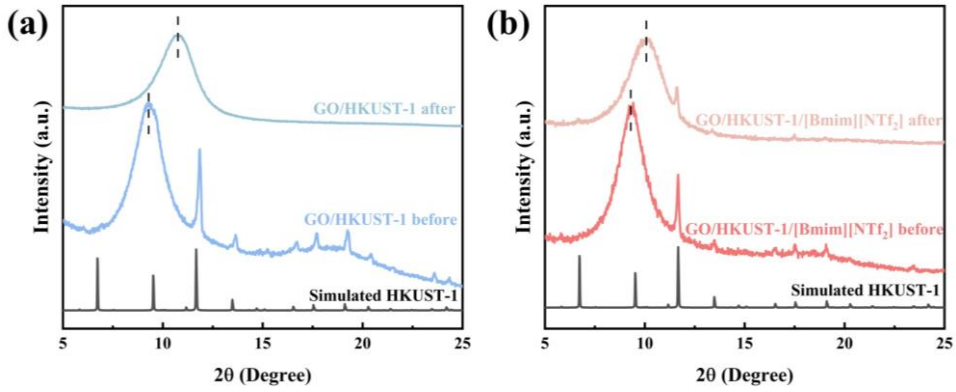


**Fig. S22** The XRD patterns of (a) GO/HKUST-1 composite membrane and (b) GO/HKUST-1/[Bmim][$NTf_2$] composite membrane before and after testing in 0.5 M NaCl solution for 11 h.

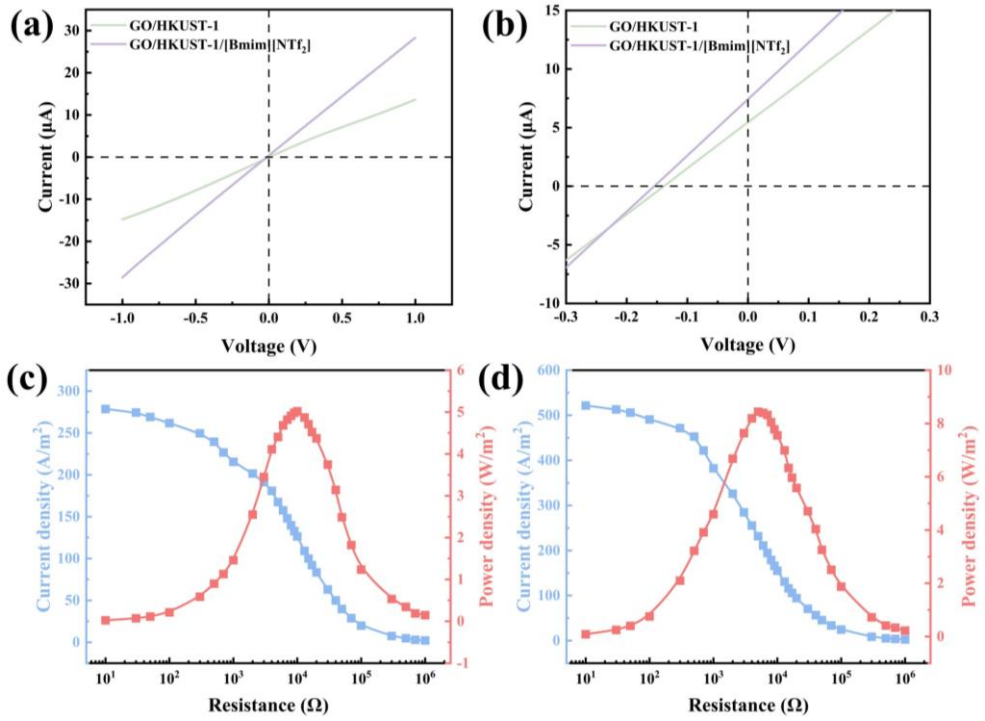


**Fig. S23** (a) The *I–V* curves of GO/HKUST-1 composite membrane and GO/HKUST-1/[Bmim][$NTf_2$] composite membrane in 0.01 M KCl electrolyte solution. (b) The *I–V* curves of GO/HKUST-1 composite membrane and GO/HKUST-1/[Bmim][$NTf_2$] composite membrane under 50-fold NaCl concentration gradient. The current density and power density of (c) GO/HKUST-1 composite membrane and (d) GO/HKUST-1/[Bmim][$NTf_2$] composite membrane with different external resistances under 50-fold NaCl concentration gradient.

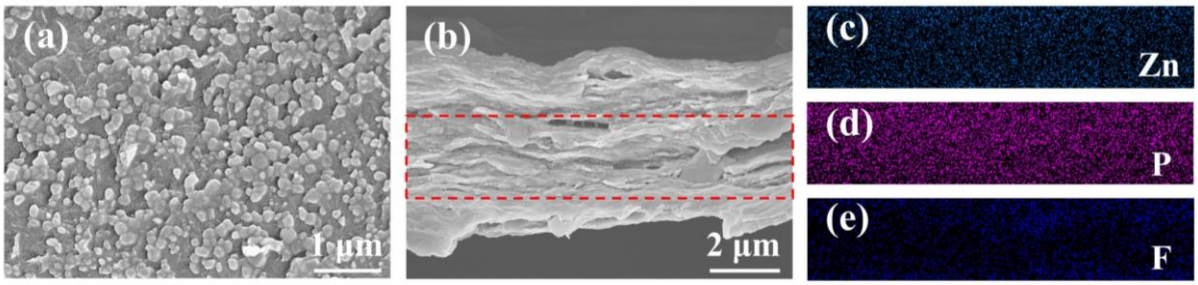


**Fig. S24** The surface (a) and cross-section (b) SEM images of GO/ZIF-8/[Bmim][$PF_6$] composite membrane. The element mapping images of (c) Zn, (d) P and (e) F of the marked section zone in (b).

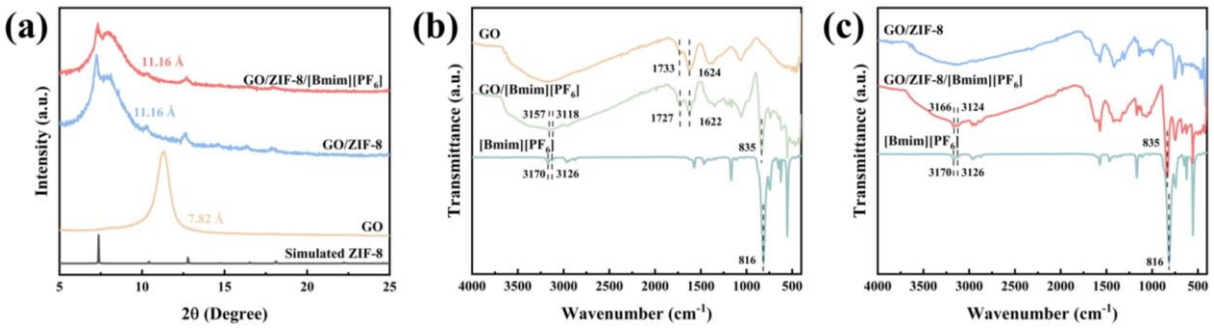


**Fig. S25** (a) The XRD patterns of GO membrane, GO/ZIF-8 composite membrane and GO/ZIF-8/[Bmim][$PF_6$] composite membrane. (b) The ATR–FTIR spectra of GO membrane, [Bmim][$PF_6$] and GO/[Bmim][$PF_6$] membrane. (c) The ATR–FTIR spectra of GO/ZIF-8 composite membrane, [Bmim][$PF_6$] and GO/ZIF-8/[Bmim][$PF_6$] composite membrane.

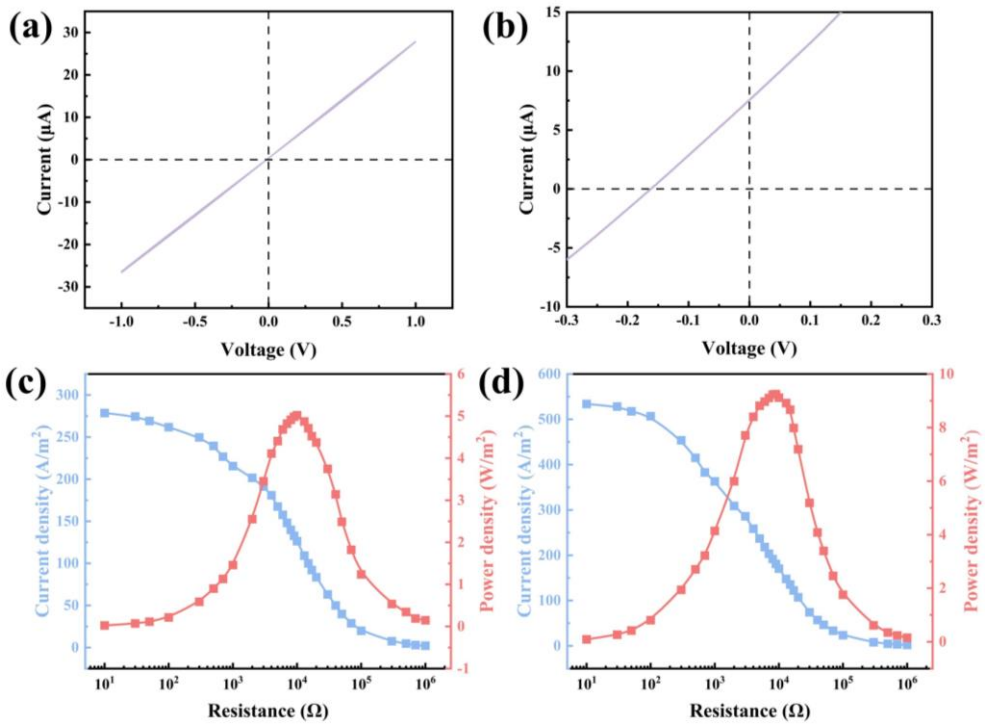


**Fig. S26** (a) The *I–V* curves of GO/ZIF-8/[Bmim][$PF_6$] composite membrane in 0.01 M KCl electrolyte solution. (b) The *I-V* curves of GO/ZIF-8/[Bmim][$PF_6$] composite membrane under 50-fold NaCl concentration gradient. The current density and power density of (c) GO/[Bmim][$PF_6$] membrane and (d) GO/ZIF-8/[Bmim][$PF_6$] composite membrane with different external resistances under 50-fold NaCl concentration gradient.

# Supplementary Tables

**Table S1** The bare ionic diameter, hydrated ionic diameter, hydration free energy and diffusion coefficient of studied ion species.[错误!未找到引用源。]

| Ion species | Bare ionic diameter (Å) | Hydrated ionic diameter (Å) | Hydration free energy (kJ $mol^{-1}$) | Diffusion coefficient ($10^{-5}$ $cm^2$ $s^{-1}$) |
|---|---|---|---|---|
| $Li^+$ | 1.20 | 7.64 | -475 | 1.029 |
| $Na^+$ | 1.90 | 7.16 | -365 | 1.334 |
| $K^+$ | 2.66 | 6.62 | -295 | 1.957 |
| $Ca^{2+}$ | 1.98 | 8.24 | -1505 | 0.792 |
| $Mg^{2+}$ | 1.30 | 8.56 | -1830 | 0.706 |
| $Cl^-$ | 3.62 | 6.64 | -340 | 2.302 |

**Table S2** The $I_{sc}$, $V_{oc}$, $E_{redox}$, $E_{diff}$, $t_+$ and $\eta$ of GO membrane under a series of NaCl concentration gradients.

| Concentration gradient (M/M) | 0.05/0.01 | 0.1/0.01 | 0.5/0.01 | 1/0.01 | 5/0.01 |
|---|---|---|---|---|---|
| $I_{sc}$ (μA) | 0.9 | 1.2 | 2.7 | 4.6 | 8.5 |
| $V_{oc}$ (mV) | 61.1 | 82.5 | 128.6 | 137.2 | 157.2 |
| $E_{redox}$ (mV) | 37.9 | 50.6 | 80.9 | 90.2 | 100.3 |
| $E_{diff}$ (mV) | 23.2 | 31.9 | 47.7 | 47.0 | 56.9 |
| $t_+$ | 0.799 | 0.790 | 0.759 | 0.718 | 0.696 |
| $\eta$ (%) | 18.05 | 16.82 | 13.42 | 9.51 | 7.72 |

**Table S3** The $I_{sc}$, $V_{oc}$, $E_{redox}$, $E_{diff}$, $t_+$ and $\eta$ of GO/ZIF-8 composite membrane under a series of NaCl concentration gradients.

| Concentration gradient (M/M) | 0.05/0.01 | 0.1/0.01 | 0.5/0.01 | 1/0.01 | 5/0.01 |
|---|---|---|---|---|---|
| $I_{sc}$ (μA) | 1.6 | 3.4 | 5.5 | 9.5 | 13.7 |
| $V_{oc}$ (mV) | 74.5 | 93.2 | 146.5 | 161.5 | 181.7 |
| $E_{redox}$ (mV) | 37.9 | 50.6 | 80.9 | 90.2 | 100.3 |
| $E_{diff}$ (mV) | 36.6 | 42.6 | 65.6 | 71.3 | 81.4 |
| $t_+$ | 0.972 | 0.887 | 0.856 | 0.831 | 0.780 |
| $\eta$ (%) | 44.54 | 30.05 | 25.37 | 21.85 | 15.74 |

**Table S4** The $I_{sc}$, $V_{oc}$, $E_{redox}$, $E_{diff}$, $t_+$ and $\eta$ of GO/ZIF-8/[Bmim][$NTf_2$] composite membrane under a series of NaCl concentration gradients.

| Concentration gradient (M/M) | 0.05/0.01 | 0.1/0.01 | 0.5/0.01 | 1/0.01 | 5/0.01 |
|---|---|---|---|---|---|
| $I_{sc}$ (μA) | 1.7 | 3.5 | 7.9 | 13.1 | 17.8 |
| $V_{oc}$ (mV) | 75.1 | 102.1 | 162.9 | 178.2 | 211.5 |
| $E_{redox}$ (mV) | 37.9 | 50.6 | 80.9 | 90.2 | 100.3 |
| $E_{diff}$ (mV) | 37.2 | 51.5 | 82.0 | 88.0 | 111.2 |
| $t_+$ | 0.985 | 0.968 | 0.945 | 0.908 | 0.883 |
| $\eta$ (%) | 47.13 | 43.83 | 39.74 | 33.33 | 29.45 |

**Table S5** Comparison of the power density of GO/ZIF-8/[Bmim][$NTf_2$] composite membrane with previously reported 2D nanofluidic and MOF-based membranes under identical testing conditions (0.03 $mm^2$ testing area, 0.5 M/0.01 M NaCl concentration gradient and neutral pH).

| Membrane | Thickness (μm) | Resistance (kΩ) | Power density (W $m^{-2}$) | References |
|---|---|---|---|---|
| BN/ANF | 1 | 10 | 5.9 | [6] |
| BP/GO | 8 | 28 | 3.4 | [7] |
| GO/SNF/GO | 5 | 32 | 5.07 | 错误!未找到引用源。 |
| GO/ANF | 2.2 | 19 | 5.06 | [8] |
| MXene/CNF | 8.6 | 15 | 4.8 | 错误!未找到引用源。 |
| $MoS_2$/CNF | 4 | 23 | 5.2 | [10] |
| iGOM | 10 | 17 | 6.78 | [12] |
| GO@IL | ~13 | 23 | 6.7 | 错误!未找到引用源。 |
| PyGO | 2 | 13 | 10.4 | 错误!未找到引用源。 |
| PSS/MOF-199 | 1.6 | ~7 | 2.87 | 错误!未找到引用源。 |
| ZnTCPP-SPEEK/SPSF | 4.3 | ~25 | 6.96 | 错误!未找到引用源。 |
| UiO-66-$NH_2$ | 0.71 | ~25 | 1.47 | 错误!未找到引用源。 |
| UiO-66-$NH_2$/ZIF-8 | 75.3 | 10 | 8.72 | 错误!未找到引用源。 |
| UiO-66-$NH_2$/BANM | 0.86 | 11.3 | 8 | 错误!未找到引用源。 |
| MXene/ZIF-8 | ~2 | 3.9 | 7.18 | [5] |
| MXene/Cu-TCPP | 25 | 9 | 8.29 | 错误!未找到引用源。 |
| ZIF-8/ANF | 4.8 | 3.9 | 7.92 | 错误!未找到引用源。 |
| GO/ZIF-8/[Bmim][$NTf_2$] | 4 | 6 | 10.4 | This Work |

## References


[1] J. Abraham, K. S. Vasu, C. D. Williams, K. Gopinadhan, Y. Su, C. T. Cherian, J. Dix, E. Prestat, S. J. Haigh, I. V. Grigorieva, P. Carbone, A. K. Geim and R. R. Nair, *Nat. Nanotechnol.*, 2017, **12**, 546–+.

[2] C.-W. Chu, A. R. Fauziah and L.-H. Yeh, *Angew. Chem., Int. Ed.,* 2023, **62**, e202303582.

[3] G. Laucirica, M. E. Toimil-Molares, C. Trautmann, W. Marmisollé and O. Azzaroni, *Chem. Sci.*, 2021, **12**, 12874–12910.

[4] C. Cheng, G. P. Jiang, G. P. Simon, J. Z. Liu and D. Li, *Nat. Nanotechnol.*, 2018, **13**, 685–+.

[5] R. K. Tonnah, M. L. Chai, M. Abdollahzadeh, H. Xiao, M. Mohammad, E. Hosseini, M. Zakertabrizi, D. Jarrahbashi, A. Asadi, A. Razmjou and M. Asadnia, *ACS Nano*, 2023, **17**, 12445–12457.

[6] J. Zhou, J. Hao, R. Wu, L. Su, J. Wang, M. Qiu, B. Bao, C. Ning, C. Teng, Y. Zhou and L. Jiang, *Adv. Funct. Mater.*, 2022, **32**, 2209767.

[7] C. Chen, D. Liu, L. He, S. Qin, J. Wang, J. M. Razal, N. A. Kotov and W. Lei, *Joule*, 2020, **4**, 247–261.

[8] Z. Zhang, P. Zhang, S. Yang, T. Zhang, M. Loeffler, H. Shi, M. R. Lohe and X. Feng, *Proc. Natl. Acad. Sci. U.S.A.*, 2020, **117**, 13959–13966.

[9] W. Xin, H. Xiao, X.-Y. Kong, J. Chen, L. Yang, B. Niu, Y. Qian, Y. Teng, L. Jiang and L. Wen, *ACS Nano*, 2020, **14**, 9701–9710.

[10] J. J. Chen, W. W. Xin, W. P. Chen, X. L. Zhao, Y. C. Qian, X. Y. Kong, L. Jiang and L. P. Wen, *ACS Cent. Sci.*, 2021, **7**, 1486–1492.

[11] P. Liu, T. Zhou, L. S. Yang, C. C. Zhu, Y. F. Teng, X. Y. Kong and L. P. Wen, *Energy Environ. Sci.*, 2021, **14**, 4400–4409.

[12] C. Zhu, P. Liu, B. Niu, Y. Liu, W. Xin, W. Chen, X.-Y. Kong, Z. Zhang, L. Jiang and L. Wen, *J. Am. Chem. Soc.*, 2021, **143**, 1932–1940.

[13] P.-P. Yan, X.-C. Chen, Z.-X. Liang, Y.-P. Fang, J. Yao, C.-X. Lu, Y. Cai and L. Jiang, *Small*, 2023, **19**, 2205003.

[14] Y. H. Hu, H. Y. Xiao, L. Fu, P. Liu, Y. D. Wu, W. P. Chen, Y. C. Qian, S. Y. Zhou, X. Y. Kong, Z. Zhang, L. Jiang and L. P. Wen, *Adv. Mater.*, 2023, **35**, 2301285.

[15] Y. Guo, X. Zhang, S. Zhou, Q. Liang, H. Zeng, Y. Xu, A. Awati, K. Liang, D. Zhu, M. Liu, L. Jiang and B. Kong, *Angew. Chem., Int. Ed.*, 2025, **64**, e202500116.

[16] R. Li, J. Jiang, Q. Liu, Z. Xie and J. Zhai, *Nano Energy*, 2018, **53**, 643–649.

[17] X. Zhao, C. Lu, L. Yang, W. Chen, W. Xin, X.-Y. Kong, Q. Fu, L. Wen, G. Qiao and L. Jiang, *Nano Energy*, 2021, **81**, 105657.

[18] L. Yao, Q. Li, S. Pan, J. Cheng and X. Liu, *Front. Bioeng. Biotechnol.*, 2022, **10**, 901507.

[19] Z. J. Yang, L. H. Yeh, Y. H. Peng, Y. P. Chuang and K. C. W. Wu, *Angew. Chem., Int. Ed.*, 2024, **63**, e202408375.

[20] W. H. Lin, T. Y. Huang, C. H. Bai, C. H. Hung, C. A. Lung, W. H. Hung, K. Gopinadhan and L. H. Yeh, *Nano Energy*, 2024, **128**, 109924.

[21] X. Zheng, X. Ma, Z. Yuan, X. Zhang, R. Zhai, R. Duan, X. Song, C. Teng, Y. Zhou and L. Jiang, *Adv. Funct. Mater.*, 2025, DOI: 10.1002/adfm.202504519.